Mon. Not. R. Astron. Soc. **314**, 702–712 (2000)

Models of the dust structures around Vega-excess stars

W. R. F. Dent,[1★] H. J. Walker,[2] W. S. Holland[3] and J. S. Greaves[3]
[1]*UK Astronomy Technology Centre, Royal Observatory, Blackford Hill, Edinburgh EH9 3HJ*
[2]*CCLRC, Chilton, Didcot, Oxfordshire OX11 0QX*
[3]*Joint Astronomy Centre, 660 N. A'ohōkū Place, Hilo, HI 96720, USA*

Accepted 1999 November 26. Received 1999 November 22; in original form 1999 August 25

ABSTRACT

We present models of the submillimetre dust emission around four Vega-excess stars. The results are adjusted to fit simultaneously the spectral energy distribution from millimetre through to optical wavelengths, as well as the submillimetre image. The combination of spatially resolved images with continuum fluxes over a range of wavelengths can remove some of the previous ambiguities in estimating the dust emission characteristics and circumstellar distributions.

Fomalhaut shows the brightest and best-resolved submillimetre image, and so gives the most unambiguous fit. Both the imaging and photometric results can best be modelled by an edge-on thick torus, of inner radius 100 au, outer radius 140 au and thickness ~120 au. The observed sharp outer boundary cannot be fitted by a reasonable power-law density distribution. Furthermore, inside 100 au the density also drops abruptly, by at least a factor of 10.

The structures of Vega and ϵ Eri are also best modelled by radially thin rings rather than discs, in both cases viewed almost pole-on. However, there are clearly clumps in their morphologies which cannot be explained by simple axisymmetric models.

The submillimetre disc in β Pic can be adequately fitted by the same model as that used to account for the extended structure seen in scattered light. However, the additional south-western emission component, if it lies in the β Pic system, must have a dust mass comparable to that of the whole visible disc.

In all cases, the spectral energy distribution can be fitted by a single ring or disc-like structure. Grain sizes of a few tens of μm and $\beta = 0.8$–1.1 provide the best fits, and we place limits on the dust size distribution.

The dust temperatures are too low and there is too much temperature variation between the sources for grain sublimation to be effective at creating the central holes. All rings are dominated by grain–grain collisions, and we discuss methods of creating and sustaining the observed structures. Most likely they arise from a mechanism such as planet shepherding. The outer cut-off may arise in a similar way, although external stripping of material is not discounted.

Key words: circumstellar matter – dust, extinction.

1 INTRODUCTION

The far-infrared excess of Vega was discovered serendipitously during *IRAS* calibration observations (e.g. Aumann et al. 1984). Follow-up studies revealed that as many as 20 per cent of main-sequence stars have such excess flux (Aumann 1985; Mannings & Barlow 1998). Assumed to be warm circumstellar dust, subsequent observations have shown that the material can also be detected from ground-based telescopes at submillimetre wavelengths (Zuckerman & Becklin 1993) and in the mid-infrared (e.g. Fajardo-Acosta, Telesco & Knacke 1998). More recent studies at far-infrared wavelengths using *ISO* have provided better constraints on the spectral energy distribution (SED) of the dust, and have been used to obtain a characteristic temperature (e.g. Heinrichsen, Walker & Klaas 1998; Dominik et al. 1998).

In a few cases (β Pictoris: Smith & Terrile 1984; 55 Cnc: Trilling & Brown 1998; HR 4796A: Schneider et al. 1999) the starlight scattered off the dust has been imaged in the optical or near-infrared using coronographs. A similarly small number of objects have also been resolved in the mid-infrared (e.g. Pantin, Lagage & Artymowicz 1997; Koerner et al. 1998), and show extended thermal emission from hot dust relatively close to the

★ E-mail: dent@roe.ac.uk

star. The advent of sensitive detector arrays operating at submillimetre wavelengths has recently produced images of more extended warm dust from the closest of the Vega-excess stars (Holland et al. 1998; Greaves et al. 1998). Both the submillimetre and mid-infrared images show material confined mostly to flattened structures, thought to be discs around the central stars. Typical sizes are tens to ~100 au, noted by Greaves et al. to be similar to that of the Edgeworth–Kuiper belt in our Solar system.

Several models using an axisymmetric optically thin radiative transfer code have been used to investigate the SEDs of these objects (e.g. Sylvester & Skinner 1996). However, apart from simulations of the scattered light and the mid-infrared emission from the β Pictoris disc (e.g. Kalas & Jewitt 1995; Pantin et al. 1997) and more recently HR 4796A (Augereau et al. 1999), there have been few detailed models of the morphology of these dust structures. This has been mainly due to the lack of spatial information and low signal-to-noise ratio at the longer wavelengths.

In the following, we have used known stellar data, together with published mid- and far-infrared fluxes (particularly from *ISO*), and submillimetre fluxes and continuum images of the 'big four' Vega-excess stars, and have attempted to construct models to fit both the observed dust structure and the SED. From these, we try to identify a unified picture of such objects. The stars investigated are Vega, Fomalhaut, β Pictoris and ϵ Eridani.

2 MODELLING

The models are adapted from a two-dimensional continuum radiative transfer program developed for protostellar discs (Dent 1988). In most cases the dust masses are such that optical depths are relatively small – even at optical wavelengths, although in the disc plane, optical extinction of up to ~1 mag may be present. Because of this, account is still taken of optical depth and cloud self-heating. The model has a logarithmic two-dimensional grid of points from 1 to 600 au in radius and distance above the plane. As will be shown later, this covers the region of detected emission.

The input parameters for the model are the stellar luminosity L_* and temperature T_*, the dust emissivity Q as a function of wavelength (for simplicity, this is assumed to be constant throughout the cloud), the two-dimensional dust density structure, the distance to the star D, and the inclination i of the disc plane to the line of sight (assumed to be the same inclination as that of the star). All the stars are nearby bright main-sequence objects, so L_*, T_* and D are accurately known. The inclination is mostly found from published stellar optical spectroscopy, although in the case of β Pic it is measured from the optical disc image. It is also estimated from some of the submillimetre images.

Table 1 summarizes the data on the four target objects, including stellar parameters and references to relevant published material.

The dust emission is characterized by a critical wavelength λ_0, and an opacity index β. The grains are assumed to be blackbodies (emissivity unity) shortwards of λ_0, where most of the stellar radiation is emitted. At millimetre and submillimetre wavelengths, the SEDs are observed to be steeper than blackbodies (see results later), so we adopt a power law for $\lambda > \lambda_0$ [emissivity Q proportional to $(\lambda/\lambda_0)^{-\beta}$]. A single characteristic grain radius $\bar{a}$ is used, although we have investigated the possibility of a distribution of sizes. The value of $\bar{a}/\lambda_0$ probably lies in the range $1/2\pi$ (the normal assumption of Mie theory with spherical grains) to 2π, depending on the grain structure. In the following we assume that this ratio is unity, so determination of Q through fitting of the dust temperature at a measured radius, together with a measurement of β, can give λ_0 and hence an estimate of $\bar{a}$.

Table 1. Stellar parameters for target objects.

Object name	Stellar type	Lum. ($L_\odot$)	Distance (pc)	Incl.(1) (°)	Refs.
Fomalhaut	A3V	13	7.7	<30	1,2
Vega	A0V	60	7.8	85±0.3	1,3,4
β Pic	A5V	8.9	19.3	<10	1,5
ϵ Eri	K2V	0.33	3.2	70±15	6,7

(1) An inclination of 90° means pole-on.
References: (1) Holland et al. 1998; (2) Walker et al. in preparation; (3) Heinrichsen et al. 1998; (4) Gulliver, Hill & Adelman 1994; (5) Heinrichsen et al. 1999; (6) Saar & Osten 1997; (7) Greaves et al. 1998.

A power law (r^{-p}) is assumed for the disc mid-plane density, with optional inner and outer boundaries, $r_{\rm in}$ and $r_{\rm out}$. In most cases, we have assumed a thin (unresolved) Gaussian density distribution perpendicular to the disc plane, with a thickness proportional to r^f; f is therefore a 'flaring index', and the disc surface density is $\propto r^{f-p}$. Except for possibly Fomalhaut, the submillimetre observations do not significantly resolve the structure perpendicular to the disc plane, so this is not a well-constrained part of the model. For most objects we therefore assume $f = 0$. However, for β Pictoris, $f = 1.3$ has been adopted, based on optical observations.

The results from the models are an SED integrated over the whole source, and images at selected wavelengths convolved with the appropriate beamsizes. We have tried to reproduce all the continuum observations as closely as possible using the simplest model. Table 2 summarizes these 'best-fitting' models for the four objects. In the following sections, we describe the individual objects, and show the results of investigations into some parameter space in order to gauge the uniqueness of the models.

2.1 Fomalhaut

Two features stand out in the observations of Fomalhaut. First, the SED has a single narrow peak in the far-infrared. Fig. 1 shows that this excess can be closely reproduced by an isothermal modified blackbody, in addition to the normal stellar photosphere. The lower submillimetre fluxes in this figure are published single-point photometric observations taken with relatively compact beams, so are likely to underestimate the total flux in such an extended double source. Since Fomalhaut is marginally resolved by *ISO* at the shorter wavelengths (Walker et al. in preparation), the data were processed using the ISOPHOT analysis package PIA v8.0. They have been colour-corrected for a modified blackbody of $T = 45$ K, $\beta = 1$, and are consistent with the *IRAS* data.

The second distinctive feature of the Fomalhaut observations is the remarkably symmetrical double-peaked submillimetre image (see Fig. 2, based on data from Holland et al. 1998). The two peaks have the same intensity to better than 3 per cent (i.e. well within the formal noise level). The peak separation is 19 arcsec, so this was reasonably well-resolved by the 13.8-arcsec beam.

In the following, we have attempted to reproduce both the submillimetre image and the SED using a single self-consistent model; we also investigate the sensitivity of the model to variations in some of the main parameters.

Table 2. Disc parameters for best-fitting models.

Object name	r_{in} (au)	r_{out} (au)	p	Incl. (°)	Dust mass (M_{lunar})	$T_{dust}(1)$ (K)	λ_0 (μm)	$\lambda_{pk}(2)$ (μm)	β	Notes
Fomalhaut	100	140	0	20	1.4	40	100	100	1.1	thickness ~ 120 au
Vega	80	120	0	85	0.2	80	70	60	0.8	(3)
β Pic	20(4)	–(6)	3(4)	<10(5)	3.0	85	10	43	0.8	
ϵ Eri	50(7)	80	0	70(5)	0.07	35	30	100	0.8	

Notes.
(1) Mean dust temperature from isothermal modified blackbody fit to excess.
(2) Approximate wavelength of peak excess flux.
(3) Inclination assumed to be 85° from optical spectroscopy – see Table 1.
(4) In the range $20 \leq r \leq 100$ au, the value of p drops to 1.8; radius of inner hole is 20 au. Values are taken from optical modelling.
(5) Value taken from optical observations.
(6) No observed outer radius.
(7) Dust with a density of 10 per cent of the outer mid-plane is also present within r_{in} – see text for details.

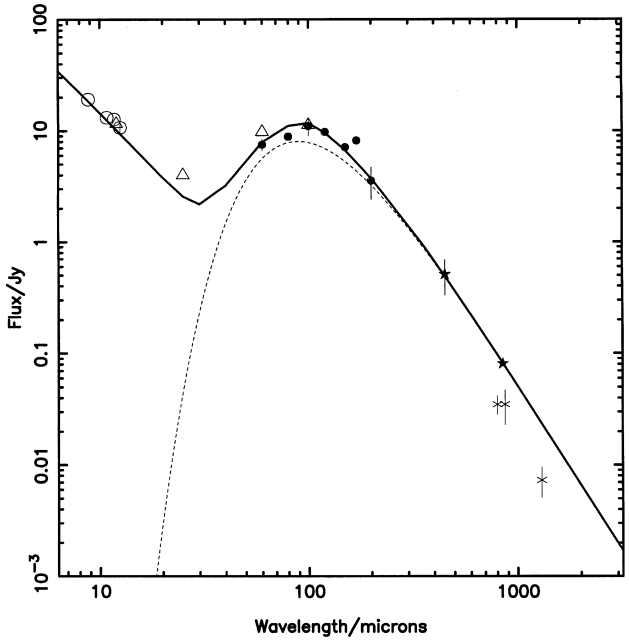

Figure 1. Continuum spectrum of Fomalhaut. Data shown are: integrated 850-μm flux from Holland et al. (1998) and 450 μm point from Holland (private communication) (filled stars); *IRAS* data from Gillett (1986) (open triangles); far-infrared points from *ISO* [filled circles; from Walker et al. (in preparation) – see text for details]; mid-infrared data from Fajardo-Acosta et al. (1998); and millimetre and submillimetre photometric points from Chini, Krügel & Kreysa (1990) and Zuckerman & Becklin (1993) (crosses). The 450-μm point represents the estimated integrated flux from low signal-to-noise ratio SCUBA mapping. Formal error bars are shown, except where these are smaller than the symbols. The solid line is the continuum spectrum of the final model for Fomalhaut (including stellar photospheric emission), and the dotted line shows a modified blackbody curve with $\beta = 1.1$ and $T = 40$ K, constrained to fit the 850-μm flux.

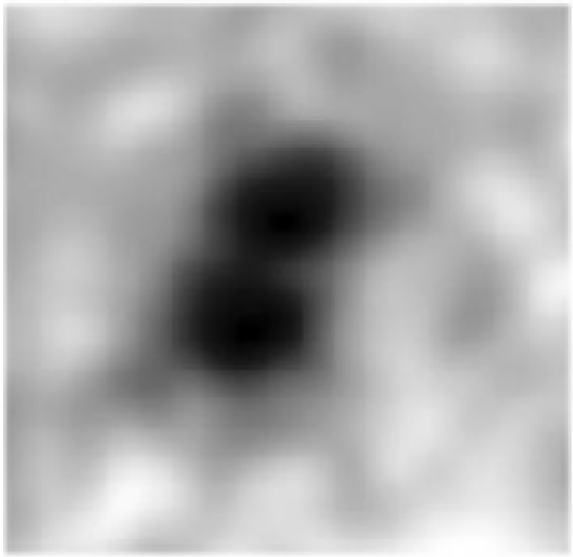

Figure 2. Observed image of Fomalhaut at 850 μm, based on data from Holland et al. (1998). The map is 90 arcsec on a side, and the star lies equidistant between the two submillimetre peaks.

2.1.1 Standard model

The near-isothermal excess and the symmetrical submillimetre morphology about the star both suggest that the dust in the Fomalhaut system has a limited range of temperature and distance from the central star. The image of Fomalhaut was interpreted by Holland et al. as an edge-on disc. We have attempted to derive quantitatively the parameters of such a model that would best fit the observed results, and the parameters for this standard model are listed in Table 2. Fig. 1 compares its continuum spectrum with published near-infrared through to millimetre-wave photometry, as well as an isothermal blackbody. Fig. 3 shows the simulated image at a wavelength of 850 μm, to the same scale as the observed data in Fig. 2.

In summary, the current simplest model for Fomalhaut consists of a torus of dust viewed nearly edge-on, with dust lying at radii of 100–140 au from the star, and a constant mid-plane density within this region. The derived radius is slightly larger than that estimated by measuring the apparent peak separation in Fig. 2, as we have taken into account the limited spatial resolution of the observations. For a marginally resolved truncated ring structure, this tends to pull the peaks together. Higher resolution submillimetre observations would be of interest: if the peak separation remains the same as in Fig. 2, this implies that the dust is located in two symmetrical clumps, rather than a ring, although the following arguments would essentially remain the same, except that the source would no longer be axisymmetric. However, the high degree of symmetry in the submillimetre image makes this rather unlikely, given that the results from theoretical models of

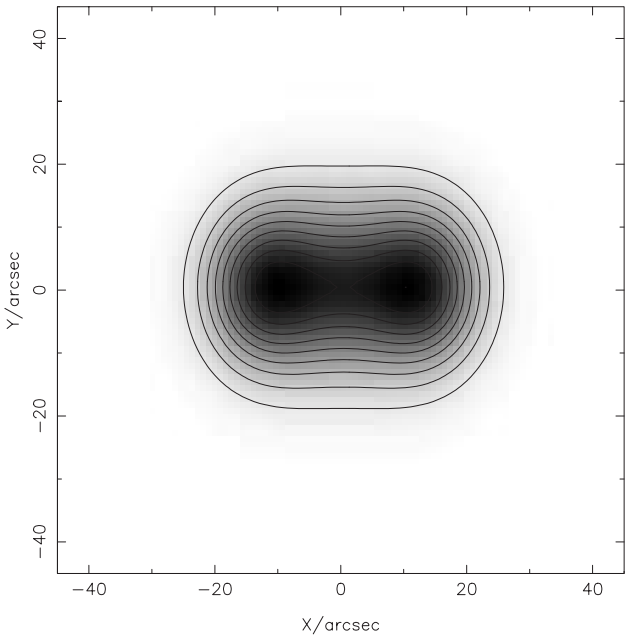

Figure 3. Standard model of the Fomalhaut circumstellar dust viewed at 850 μm, convolved with a 13.8-arcsec beam. The torus is viewed 20° out of the plane. Contour levels are 10, 20, …, 100 per cent of the peak flux.

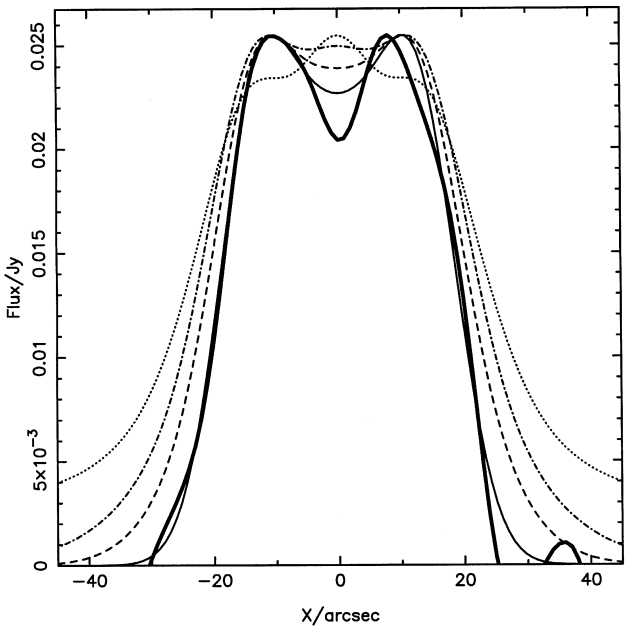

Figure 4. Cross-cut through the major axis of the 850-μm image of Fomalhaut (solid thick line) compared with various disc models. Plots are shown for models with power-law density indices (p) of 4 (dashed line), 3 (dash–dot) and 2 (dotted line). Also shown is the standard model, with $p = 0$ and an outer boundary of 140 au (solid thin line). All fluxes have been normalized to the peak observed value, and all models have the same inner hole and a disc inclination of 20°, and are convolved with a 13.8-arcsec beam. The rms errors on the observed fluxes are 4 mJy per beam (from Holland et al. 1998).

planetary systems do not produce such simple dipole dust distributions (see discussion). Preliminary SCUBA results at 450 μm with higher spatial resolution indicate that dust is indeed found between these peaks and the central star, which confirms the more axisymmetric interpretation of the structure.

2.1.2 *Outer cut-off*

The standard model for Fomalhaut has a sharp outer boundary in the dust distribution at a radius of 140 au. We can investigate whether this is truly a step function by comparing the image with models having power-law distributions. The presence of outer cool dust does not strongly affect the integrated SED, but the submillimetre image will appear significantly more extended. Parametrizing the disc mid-plane density by a power law ($n_{\rm d} \propto r^{-p}$), Fig. 4 compares a cut through the major axis of the 850-μm image with various power-law models, and also the standard model using $r_{\rm out} = 140$ au.

Fig. 4 indicates that, unless the disc density drops very rapidly (i.e. $p \geq 4$), the sharp outer edge of the submillimetre image cannot be reproduced. We conclude that the dust ring around Fomalhaut most likely has an abrupt outer boundary at a radius of 140 au. Similar models with $r_{\rm out} = 120$ or 160 au do not fit the width of the observed submillimetre image, which gives an indication of the uncertainty in this value. The origin of this outer boundary will be discussed later.

2.1.3 *Inner hole*

The 850-μm image indicates that the circumstellar dust around Fomalhaut has an evacuated inner region. The radius of this cavity is 100 au, with an error of ±10 au estimated by comparing the models with cross-cuts along the major axis of the image – in particular trying to reproduce the separation of the peaks (see Fig. 4). However, the relatively deep central 'hole' is difficult to reproduce, even with a completely evacuated central region. One possible explanation is that the disc plane is slightly inclined to the line of sight; an inclination of 20° would increase the observed depth of this hole, and is within the limits estimated from the submillimetre image (see Fig. 3, and next section).

Fig. 5 compares the SED of Fomalhaut with models having various mid-plane densities in the inner region ($r < r_{\rm in}$). Models range from an inner mid-plane density of 100 per cent of the outer value (i.e. a filled disc rather a ring), decreasing to 10, 1 and 0 per cent (i.e. an empty inner hole). Including the flux calibration uncertainty, this result indicates that the mid-plane density at $r < r_{\rm in}$ must be no more than 10 per cent of the density outside this radius. This limit is also consistent with the hole in the centre of the submillimetre image.

The absence of significant inner dust and the relatively low temperature of the ring material around Fomalhaut have implications for potential mid-infrared observations. In particular, the model predicts a relatively low surface brightness at 20 μm, of less than 25 mJy arcsec^{-2}. However, because of the steep slope on this – the Wien side of the emission curve – the disc will be significantly brighter at the longer wavelength end of the mid-infrared. For example, the disc flux at 30 μm will be more than an order of magnitude higher than at 18 μm.

2.1.4 *Ring inclination and thickness*

It was suggested by Holland et al. from the submillimetre image that the Fomalhaut ring is viewed very nearly edge-on. Cross-cuts perpendicular to the major axis through the northern peak, the central saddle and the southern peak show full widths at half-maximum of 20.0, 21.0 and 22.9 arcsec respectively. A disc

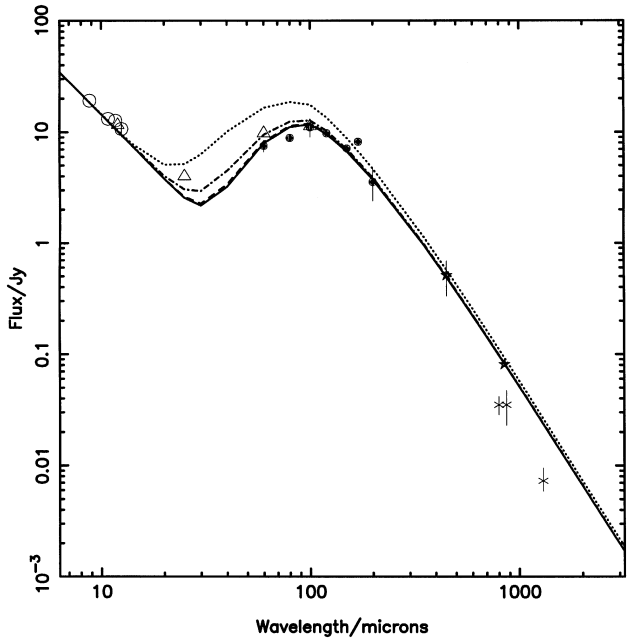

Figure 5. Continuum spectrum of Fomalhaut (data points) compared with various inner disc densities. Plots are shown for models with an inner mid-plane density of 0 per cent (solid line), 1 per cent (dashed), 10 per cent (dash–dot) and 100 per cent (dotted line) of the outer mid-plane density. All models cut off at an inner radius of 1 au.

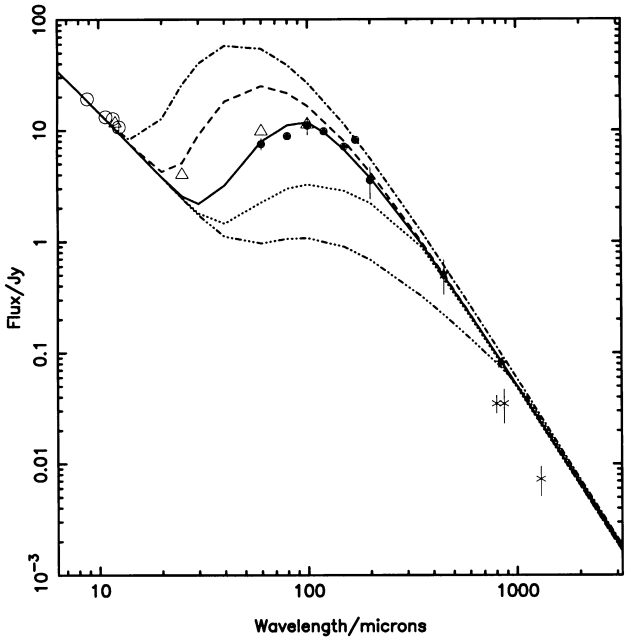

Figure 6. Continuum spectrum of Fomalhaut (data points) compared with various dust models. Plots are shown for models with dust sizes of 1000 μm (dashed line), 300 (dash–dot), 100 (solid line), 30 (dotted) and 10 μm (dash–triple-dotted line). All models have the same total dust mass.

slightly inclined to the line of sight would be expected to show wider emission in the central saddle compared with the edges. This is not seen in the above results; including estimated uncertainties, the saddle width is <5 arcsec larger than the peak widths. The observed ring diameter is 19 arcsec, implying an upper limit to the inclination i of $\sim\sin^{-1}(5/19)$, or 15°. The inclination has a negligible effect on the SED, as the optical depth is small. An accurate estimate of i must, therefore, await higher resolution data, such as a 450-μm SCUBA image.

The diffraction-limited telescope beam is 13.8 arcsec, considerably less than the observed minor axis noted above. There is no evidence that the resolved thickness result from errors in pointing or the map reconstruction algorithm, implying therefore that the dust is significantly extended above the plane. Assuming a Gaussian distribution perpendicular to the plane, the deconvolved thickness is 16 arcsec, or ∼120 au (FWHM), making the structure a thick torus rather than a disc. A possible explanation for this is noted in the discussion below.

2.1.5 Dust characteristics

The apparently close single-temperature fit and the narrow range of distances from the star where dust is located suggest that the grains around Fomalhaut may have a rather limited range of emission characteristics. As the ring is optically thin, the energy balance is dominated by radiation from the central star. The grains in the ring are likely to have a single value of emissivity ($Q_{\rm fir}$) at the wavelength of peak emission (∼100 μm), otherwise a range of temperature would be seen, thus widening the peak in Fig. 1. In Fig. 6 we compare the SEDs from equal masses of dust with various single grain sizes (assuming $\bar{a} = \lambda_0$ – see Section 2), and with the same value of β. Only the 100-μm grains will fit the observed peak. Note that, for $\beta \sim 1$, the value of the mm-wave mass opacity $\kappa_{\rm mm}$, is approximately constant within the range of $\bar{a}$ shown.

Fig. 6 indicates that the mass of grains smaller than 100 μm must be negligible, otherwise their emission would dominate the short-wavelength side of the emission. We can place an upper limit to the mass of 10-μm grains of ≤10 per cent of that at 100 μm. Secondly, the total mass of grains of size $100 < \bar{a} \leq 1000$ μm must also be less than that of $\bar{a} \approx 100$ μm grains, otherwise the spectrum will be distorted at longer wavelengths (assuming that $\bar{a}/\lambda_0 \sim 1$ – see above). Emission from the same mass of grains with $\bar{a} > 1000$ μm, however, would be negligible, so we are unable to put strong constraints on the mass of such material.

The standard Mathis–Rumpl–Nordsieck (MRN) size distribution has $m(a)\,{\rm d}a \sim a^{-0.5}$ (Mathis, Rumpl & Nordsiek 1977). The models indicate that not only must there be a sharp cut-off at $\bar{a} < 100$ μm, but also the mass of grains a few times larger than this cannot be significantly greater than for an MRN distribution. Although there are caveats about the derivation of the exact value of $\bar{a}$ from λ_0, the results do indicate a rather sharp drop in the grain size distribution rather than a monotonic slope. This has implications for the grain formation and destruction mechanisms, to be discussed later.

In the dust around some protostellar objects, the value of β may be significantly higher than a single-component fit to the SED might suggest, as it is formally possible to produce a shallow long-wavelength spectral slope with high-β grains having a range of temperature. This might occur either if the grains are distributed over a range of distances from the heating source, or there is a mixture of grain size. However, in the case of Fomalhaut, neither of these is thought to be the case. The source size estimated from analysis of the far-infrared observations (e.g. Gillett 1986) is very similar to that imaged in the submillimetre, indicating that any dust must be intermixed. Furthermore, it would require some

grains to have temperatures as low as 20–30 K (with $\beta \sim 2.0$), a factor of 2 lower than the temperature of a blackbody at the radius of the observed dust ring.

2.2 Vega

Vega was imaged with SCUBA at 850 μm (Holland et al. 1998), and far-infrared fluxes from *ISO* have been published (Heinrichsen et al. 1998). The submillimetre image shows an elongated structure, possibly double-peaked in the highest contours. However, as noted by Holland et al., it is clearly less symmetrical than Fomalhaut. Furthermore, the lower contour levels actually show a circular morphology – more indicative of a disc viewed pole-on. This is consistent with the *IRAS* 60-μm profiles (Gillett 1986). Optical spectroscopic observations of Vega itself also indicate that the star is viewed nearly pole-on (see Gulliver et al. 1994), and the lack of detectable reddening implies negligible intervening dust. An alternative model to account for the more circular outer 850-μm contours is a less inclined but highly flared disc, or perhaps a spherical dust halo with an embedded edge-on disc. Although we cannot discount the latter, it has proved difficult to reproduce the submillimetre morphology with any form of simple edge-on disc, and a pole-on orientation with a somewhat clumpy ring is the favoured explanation.

We have carried out similar modelling to that described above, and tried to fit both the SED and the general submillimetre structure. Fig. 7 compares the observed and model SEDs. Note that the *ISO* fluxes have been re-calibrated in the same way as described above for Fomalhaut. As with Fomalhaut, the excess can be closely fitted by an isothermal modified blackbody, suggesting that the dust arises from a limited range of radii from the central star (i.e. there is a central evacuated region), and that there is a limited range of grain size around Vega.

Assuming an almost face-on disc, we compare annular integrations of the observed brightness with a cross-cut through the best model in Fig. 8. Although this smooths out the effect of the asymmetric clumps in the Vega disc, the comparison can still be used to show that there is a central hole, and to estimate the inner and outer disc boundaries, listed in Table 2.

Note that the lack of a clear central peak in the submillimetre emission might account for the ambiguity in the original *IRAS* Point Source Catalog (PSC) position. Assuming that the disc is almost face-on, the density enhancements required to give the observed clumps in Vega are ~2. Possible explanations for such clumping are outlined in the discussion. Further high-resolution imaging in the submillimetre or in the mid-infrared should help to determine the detailed structure. The predicted brightness of the ring at 20 μm is $\sim 10\,\mathrm{mJy\,arcsec^{-2}}$.

2.2.1 *Constrained parameters*

The inner cut-off of the Vega disc cannot be significantly smaller than 80 au, otherwise the submillimetre profile becomes too centrally peaked, and the SED too bright in the mid-infrared. The outer cut-off cannot be greater than 120 au, otherwise the submillimetre profile becomes too wide.

The dust size must be in the range $30 < \bar{a} < 200\,\mu\mathrm{m}$, to reproduce the observed dust temperature and ring radius. Again, the mass of small grains (~10 μm) must be ≤10 per cent of that of the 70-μm grains. These results are consistent with lower limits on

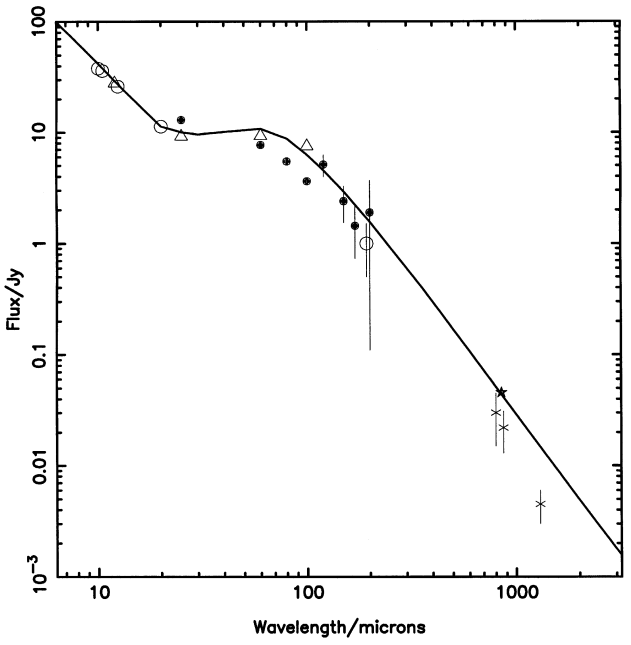

Figure 7. Continuum spectrum of Vega (data points) compared with the final model. The upper 850-μm point is integrated emission from Holland et al. (1998), and other submillimetre data are single-position photometric observations from Chini et al. (1990) and Zuckerman & Becklin (1993). Revised *ISO* fluxes are shown by filled circles, and were reduced in the same way as for Fomalhaut (see text for details). The single 193-μm point (open circle) is from Harper, Loewenstein & Davidson (1984), the *IRAS* data (open triangles) are from Gillett (1986), and the mid-infrared data are from the SIMBAD data base.

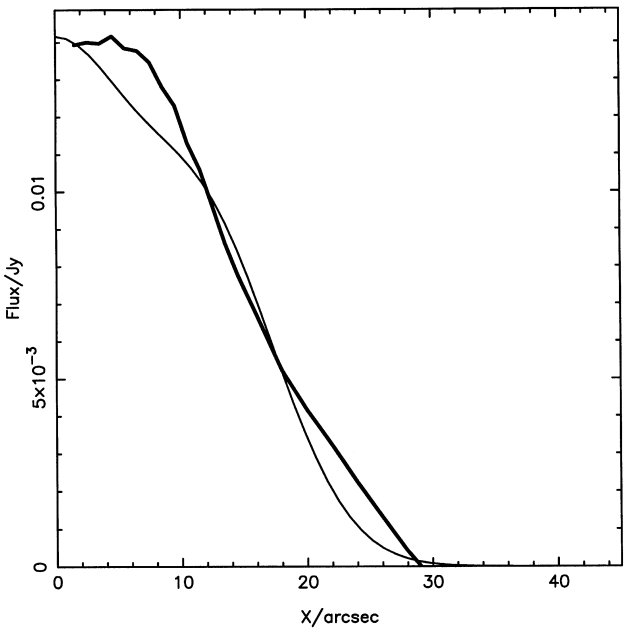

Figure 8. Azimuthally averaged radial profile of the 850-μm image of Vega (thick line) compared with the model, viewed pole-on ($i = 90°$). The peak in the centre of the model ($x = 0$) is due partly to the contribution from the stellar photosphere. For comparison, van der Bliek, Prusti & Waters (1994) estimated a diameter of 35 ± 5 arcsec from the *IRAS* 60-μm pointed observations.

the grain size of 5–10 μm, deduced from optical observations (Mauron & Dole 1998).

The model for the Vega disc is less well-constrained than that for Fomalhaut, partly owing to the lack of published photometry between 25 and 60 μm, and the relative weakness and small extent of the submillimetre emission. However, the size of the model ring is consistent with detailed interpretation of 60-μm *IRAS* pointed observations (van der Bliek et al. 1994). Also the SED can be fitted in a single-component model (Fig. 7). These results imply that the excess emission from the mid-infrared to the submillimetre can be accounted for by a single physical structure, likely to be a pole-on ring of dust.

2.3 β Pictoris

This object provided the first image of scattered light from the dust around a main-sequence star (Smith & Terrile 1984). Models of the optical and near-infrared profiles indicate a mid-plane density which decreases as r^{-3} from radii of ∼100 au (5 arcsec) out to ≥700 au (Kalas & Jewitt 1995), with no evidence of an outer cut-off. Within 100 au, the slope p decreases to ∼1.8, and an inner cavity of radius ∼20 au is indicated by the *IRAS* SED (e.g. Backman & Paresce 1993), although this inner structure is not resolved by the submillimetre observations. The submillimetre image taken by Holland et al. shows a second component to the south-west; however, no evidence was found for an optical counterpart.

Mid-infrared images have been obtained by Pantin et al. (1997) at 10 μm and by Heinrichsen et al. (1999) at 25 and 60 μm using *ISO*. The former high-resolution image (beamsize approximately 0.33 arcsec) shows only the inner disc, with a total observed diameter of ∼10 arcsec; Pantin et al. modelled this by assuming that the emission only comes from silicate grains in the inner low-p region (within ∼100 au). The *ISO* data have a significantly larger beamsize, but were processed to obtain higher effective resolution, and show emission with a major axis of ∼16 arcsec to the lowest contour. By comparison, the submillimetre image is considerably larger, with a full width of ∼44 arcsec. Does this mean that an extra dust component is required for the submillimetre emission, or can the density distribution derived from the optical and mid-infrared images account for the submillimetre extent?

We have taken the Kalas & Jewitt density model and applied it to the submillimetre image and SED. A single-component dust model has been used, with $\beta = 0.8$ and $\bar{a} = 10$ μm required to fit the observed SED at the longer wavelengths. Extensive mid-infrared spectroscopic and photometric observations have shown evidence of silicate and possibly multi-component dust grains (e.g. Knacke et al. 1993; Li & Greenberg 1998). We make no attempt here to provide detailed fits at these wavelengths, but simply ensure that our model can reproduce the average mid-infrared flux. Fig. 9 compares the observed SED with the model. The 850-μm point is the integrated emission within a radius of 30 arcsec and ignores the south-western compact source (see Heinrichsen et al.). The resultant 850-μm cross-cut along the major axis is shown in Fig. 10. Although the model slightly overestimates the flux around 200 μm, it does reproduce, within the errors, both the SED and the observed width of the central disc in β Pic. This indicates that no extra cool disc component is required outside the optically imaged dust region. Furthermore, if different dust components are responsible for the scattered optical light and submillimetre emission, they must be closely intermixed within the disc.

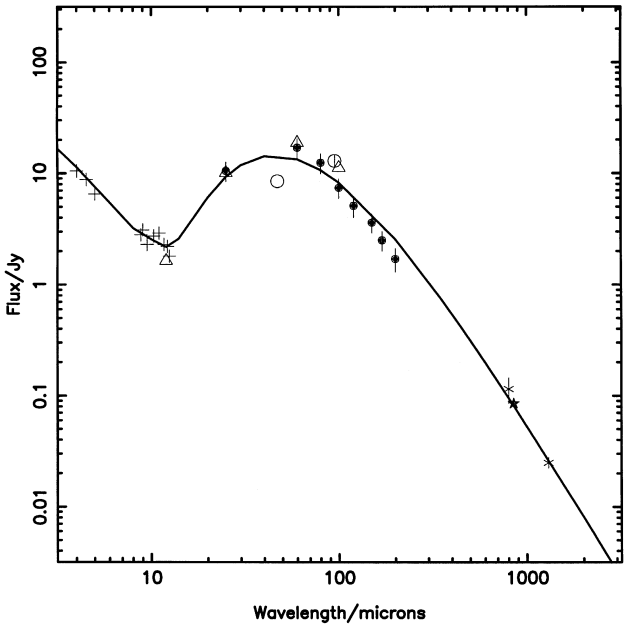

Figure 9. Continuum spectrum of β Pic (data points) compared with the model. The integrated 850-μm flux from Holland et al. (1998) is shown as a filled star. Other millimetre and submillimetre fluxes are from Chini et al. (1991) and Zuckerman & Becklin (1993). Also shown are the *ISO* data from Heinrichsen et al. (1999), *IRAS* PSC fluxes (open triangles) and 47- and 95-μm fluxes from Harvey et al. (1996), shown as open circles. The mid-infrared fluxes are from Telesco & Knacke (1991) and Knacke et al. (1993).

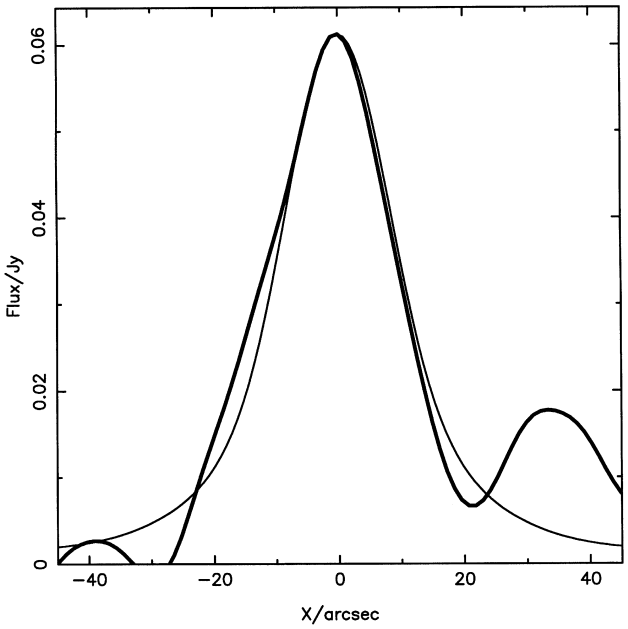

Figure 10. Cross-cut through the major axis of the 850-μm image of β Pic (thick line) compared with the model. The cut through the data has been taken at the same position angle as the optical disc, and clearly shows the additional component at a distance of ∼ +35 arcsec. See text for more details.

It is clear from the image and cross-cut at 850 μm that an additional compact source lies 35 arcsec to the south-west of β Pic

(see Fig. 10). Holland et al. (1998) have discussed the possible origins of this emission; we have taken further SCUBA data and confirmed its flux at 850 μm as 24 ± 5 mJy, and have ruled out a counterpart on the opposite side of the star down to a 1σ noise level of 2 mJy beam^{-1}. Assuming that the south-western clump lies in the β Pic system, has the same dust characteristics as the submillimetre disc, and is heated by the central star, then the mass would be 1.2 M_{lunar} – comparable to the mass of the whole visible disc. This tends to rule out an association with the β Pic system, as there is no evidence for this structure in deep optical images.

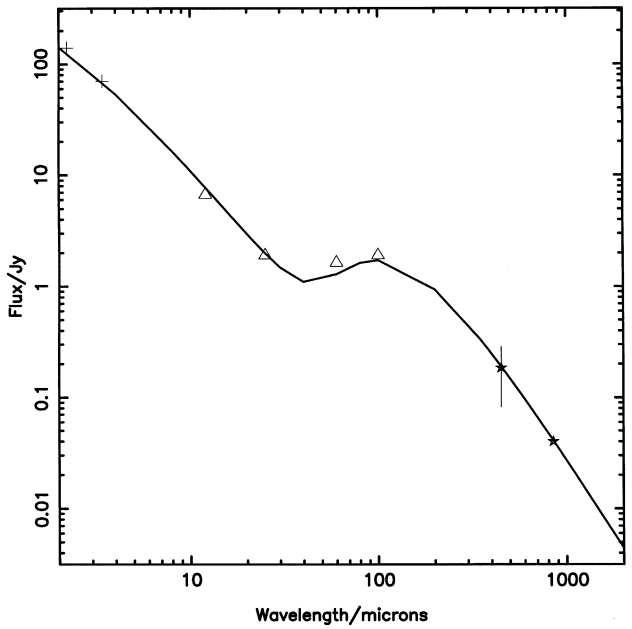

Figure 11. Continuum spectrum of ϵ Eri (data points) compared with the model. Fluxes are obtained from Greaves et al. (1998), the *IRAS* PSC (shown by triangles), and the SIMBAD data base.

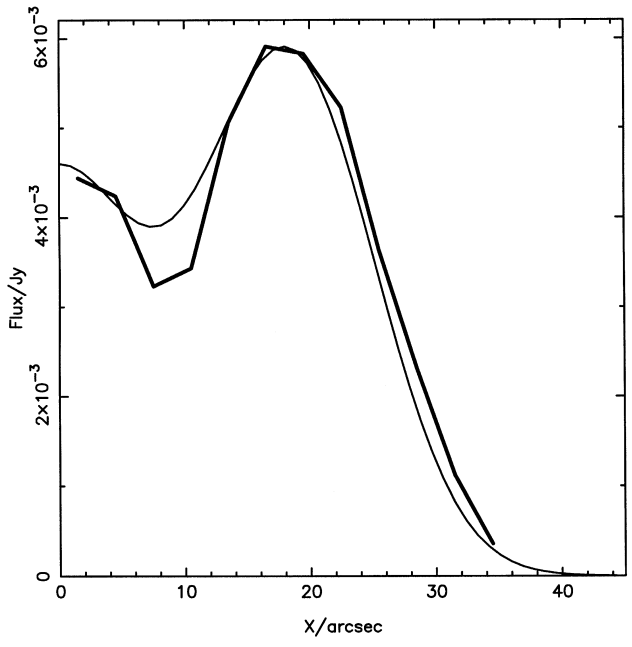

Figure 12. Azimuthally averaged radial profile of the 850-μm image of ϵ Eri (thick line) compared with the model. See text for details.

2.4 ϵ Eridani

The dust around this star was first imaged by Greaves et al. (1998). They suggested that the material lies in a ring viewed almost face-on. A complicating factor is the clumpy flux distribution, with at least two clearly identified peaks at similar radii from the star. For the present modelling, we have just assumed a two-dimensional structure.

Figs 11 and 12 compare the spectrum and azimuthally averaged flux distribution of ϵ Eri with those of the model. The best-fitting model has a narrow ring of dust at 50 to 80 au from the star; other parameters are summarized in Table 2. In addition to the ring, a second low-density dust component is required to produce the weaker 850-μm emission from near the star. This has a mean density ~10 per cent of that at $r \geq 50$ au to reproduce the observed cross-section and SED, with an innermost cut-off of 10 au (althought the latter is not well-constrained). High-resolution mid-infrared imaging would be of interest, as this inner material may correspond to the hot inner grains in the β Pic system. Similarly to the models of Fomalhaut and Vega, the main ring in ϵ Eri has sharp inner and outer boundaries.

3 SUMMARY OF THE RESULTS: A UNIFIED MODEL?

The models of the four Vega-excess stars at first present a rather disparate set of results. In particular, the dust around Fomalhaut, Vega and ϵ Eri appears to trace a torus rather than the radially extended disc structure seen in β Pic. However, the objects do have some common features.

(i) All have sharply defined central cavities, of radii 20–100 au.

(ii) Grain sizes are relatively large, 10–100 μm, with β in a narrow range from 0.8 to 1.1.

(iii) Dust masses are typically ~M_{lunar}.

(iv) Three have sharp outer boundaries, of radii 80–140 au, implying that the dust lies in sharply defined rings, rather than discs. This is also seen in the recent *HST* near-infrared image of HR 4796A (Schneider et al. 1999).

(v) The two face-on rings have bright spots, presumably caused by dust density enhancements of a factor of ~2. The other two are viewed edge-on, making it difficult to identify such clumps if they exist.

In the following, we discuss possible origins of some of these generic features.

3.1 Grain size

It is clear from published papers that using observed SEDs to determine realistic grain structures and compositions is a difficult problem (e.g. Krügel & Siebenmorgen 1996, and references therein). This is potentially complicated in the Vega-excess stars because the derived values of λ_0 for all four objects are in the range 10–100 μm, which is similar to the wavelength of peak emission (λ_{pk}). The simple power-law emissivity dependence for dust will break down when $\lambda \sim \bar{a}$: for example, Krügel & Siebenmorgen indicated a significant increase in the mass absorption coefficient (which is $\propto Q$) for $\bar{a}/\lambda = 0.1$–1.0. Table 2 shows that $\lambda_0/\lambda_{pk} = 0.25$–1.2 for the observed objects. Despite this, the fits to the SED indicate a rather smooth and shallow slope, with in all cases $\beta = 0.8$–1.1. This would indicate either

Table 3. Comparison of time-scales for Vega-excess dust rings.

Object name	Stellar age (yr)	τ_{PR} (yr)	τ_{coll} (yr)	$a_{cr}(3)$ (mm)	Refs.
Fomalhaut	2×10^8	2×10^8	2×10^5	11	1
Vega	2×10^8	2×10^7	5×10^5	3.8	1
β Pic(1)	8×10^7	2×10^7	2×10^4	2.5	2
ϵ Eri	$5–10\times10^8$	7×10^8	1×10^7	0.5	3
HR 4796A(2)	8×10^6	2×10^6	1×10^3	4.0	4,5

Notes.
(1) Values are calculated at a radius of 100 au, the transition point between the shallow ($p = 1.7$) and steep ($p = 3$) density gradients in the disc.
(2) Time-scales are from Augereau et al. (1999).
(3) Minimum dust size for survival against grain–grain collisions within the stellar lifetime. See text for details.
References: (1) Barrado y Navascués 1998; (2) Backman & Paresce 1993; (3) Greaves et al. 1998; (4) Augereau et al. 1999; (5) Stauffer, Hartmann & Barrado y Navascués 1995.

that the grain model predicting these resonances is inapplicable, or that the grain size $\bar{a} < \lambda_0$. Furthermore, the optical albedo of these large grains may be high, so they absorb less stellar radiation than assumed and could be cooler than a blackbody. This would result in an overestimate of $\bar{a}$. One must be mindful of these uncertainties in $\bar{a}$ in the following discussions.

Backman & Paresce (1993) suggested that the large size of grains around Vega, Fomalhaut and β Pic may be due to expulsion of the smaller particles through radiation pressure. However, this is unlikely to be the only factor. The critical parameter determining the grain blowout size is L_*/M_*; for ϵ Eri, this is 100 times smaller than for Vega. In this ring, only sub-micron grains could be expelled by this means, yet the grains around ϵ Eri are very similar in size to those around the luminous A-type stars (see Table 2). More accurate mid-infrared photometry would be of interest to search for the existence of warmer grains in this ring.

Poynting–Robertson (P–R) drag would also tend to remove smaller particles. While the grain sizes are large compared with typical interstellar dust, it was also pointed out by, for example, Backman & Paresce (1993) that, in the inner regions of discs around the three A-type stars, the grains are still not large enough to be stable against the P–R effect. In the ring models of these objects as described above, the disc radius and grain size are better constrained, so we have re-assessed the grain removal time-scales in light of these results. Table 3 compares the estimated stellar ages with the P–R time-scales. Also included are values for the denser ring system around the younger star HR 4796A, given by Augereau et al. (1999). In all cases except possibly ϵ Eri and Fomalhaut, the dust rings should not survive for the age of the star. Although even micron-sized grains would be just P–R stable in these two rings, the values of λ_0 and hence $\bar{a}$ (Table 2) are as large as those around the other stars, suggesting that P–R drag is not the only mechanism affecting the average grain size in these systems.

3.2 Origin of the dust rings

It was known from the low mid-infrared fluxes in the SEDs of Vega-excess stars that many are depleted of dust in the region near the centre (e.g. Chini et al. 1991). A common feature of models of the resolved dust structures described above is that the inner boundaries appear to be abrupt. A similar sharp inner boundary is also seen in the optical image of HR 4796A (Schneider et al. 1999; Augereau et al. 1999). In all except β Pic, there is also an abrupt drop-off in the dust density at large radii. The fact that such sharp inner and outer boundaries are seen in four and possibly five out of five spatially resolved objects with a wide variety of ages indicates that they are common throughout the life of these systems. These rings could be caused either by removal of grains from from all except a favoured radius, or by the formation or trapping of excess grains in this region.

Several effects can remove grains from the inner radii, including radiation pressure, P–R drag, grain collisions, sublimation and interaction with larger bodies (e.g. Zuckerman & Becklin 1993; Backman & Paresce 1993; Liou & Zook 1999). Grains can also be replenished from comets (e.g. Li & Greenberg 1998), from collisional destruction of larger grains, or from asteroids or other Edgeworth–Kuiper belt objects (e.g. Liou, Zook & Dermott 1996). The situation is likely to be a complex interplay between these phenomena, although we can estimate the relative importance of each in the rings.

(i) Radiation pressure is clearly an important factor in removing small ($\bar{a} \leq$ a few μm) particles (e.g. Backman & Paresce 1993), although it will not produce a sharp boundary, and cannot be effective for the low-luminosity stars (see above).

(ii) P–R drag is potentially important (see Table 3), but if it were the only factor involved, it would tend to create a $1/r$ density distribution and an increase in $\bar{a}$ towards the central star (Roques et al. 1994).

(iii) Liou et al. (1996) suggested that collisions with sub-micron interstellar dust can also shatter grains larger than $\bar{a} = 9\,\mu$m, although Artymowicz (1996) noted that radiation pressure can prevent this from happening around A-type stars.

(iv) Although sublimation could produce a sharp inner boundary, grains with water ice mantles normally sublimate at temperatures of ~100 K, so the rings are generally too cold for this to be effective. Furthermore, there is a much larger range of temperatures between different objects (Table 2) compared with the range within any one object (the SEDs can typically be fitted by an isothermal spectrum). The fact that sublimation is a very rapid function of temperature would argue against this effect having an important role in determining the ring structures in all these systems.

(v) Grains released from the evaporation of comets are thought to have sizes of a few μm or greater (e.g. Li & Greenberg 1998), so this might be a possible source in warm environments such as the inner region of β Pic. However, the dust torii around the other three stars are too cool for comets to evaporate significantly, unless mainly driven by species such as CO. No evidence has been found for warm CO in any of the rings (e.g. Dent et al. 1995; Greaves et al. 1998). In any case, dust production rates from comets have been measured to be $\propto r^{-1.7}$, where r is the heliocentric distance (e.g. Jewitt & Matthews 1999), so one would expect more grains at smaller radii.

(vi) The time-scales for grain–grain collisions are significantly less than the P–R drag time-scale. These values are given in Table 3 [see Backman & Paresce (1993) for calculation method]. This shows that, in all cases, collisions will dominate the removal processes of such grains from the rings. Furthermore, collisions of even larger grains ($\bar{a} \geq 100\,\mu$m) are required to replenish the observed population.

The most likely explanation for the ring structures is thought to be a massive body sweeping up grains at the inner radii. Numerical simulations by Roques et al. (1994) and Liou & Zook (1999) have produced sharp inner edges in the dust density distributions owing to mean motion resonances between the outer

planets and dust subject to P–R drag. Resonances can also provide a natural explanation for the density clumps seen in at least two of the rings. The presence of massive bodies may also prevent ring structures such as those of Fomalhaut from flattening with time, in a similar way to that in which the large inclinations of Edgeworth–Kuiper belt objects are maintained (e.g. Jewitt, Luu & Chen 1996). This might explain the apparent thickness of the toroidal structure.

One difficulty with this model is that the collisional time-scales given in Table 3 imply that grain–grain collisions would effectively remove the dust before the ring-like resonances could appear. However, the dust is likely to be replenished in a collisional cascade. If we assume an MRN size distribution (as might be the case for collisionally distributed dust), then $n(a) \propto a^{-3.5}$. For this distribution then $\tau_{\rm coll} \propto a^{1.5}$, assuming that collisions between grains of similar size are the most important. With this collisional cascade of dust, there exists a critical grain size ($a_{\rm cr}$) which will survive for the stellar age and may be the parent replenishment source of the observed grains. In all objects, this size is a few mm (Table 3). This reservoir of material may be shepherded by the planet or planets, and the smaller observable grains result from the collisional cascade within the rings.

As Fomalhaut is viewed edge-on, it might be a good candidate for the detection of radial motion owing to massive planets. However, planets associated with the dust ring will be difficult to detect in this way, owing to their large orbital period ($\sim 10^3$ yr).

3.3 Origin of the sharp outer boundaries

Apart from β Pic, the dust structures can most easily be modelled by rings with sharp outer edges. This may be a byproduct of the resonances producing the inner edge, mentioned above. The models of Roques et al. suggest that, in order to create the deep central hole and the sharp outer boundary simultaneously in a dust ring, a planet of a few Earth masses is required at the inner boundary. Their results suggest that it cannot be significantly different in mass from this, otherwise the sharp ring-like structure will be lost. Such planets must either form closer to the star and migrate outwards (e.g. Lin & Papaloizou 1986), or form at distances between 20 and as much as 100 au from the central star within the stellar age (typically 200 Myr, but as short as 8 Myr in the case of HR 4796A). It is interesting to note that the models of Stern & Colwell (1997) indicate that it may be possible to form bodies approaching this mass in the outer regions of young solar systems.

Sharp outer boundaries of radii $\sim$50 au have also been observed around the young circumstellar discs seen in silhouette in the Orion nebula (McCaughrean & O'Dell 1996). In this case, they are thought to be caused by photoevaporation owing to an OB star elsewhere in the cluster, and Störzer & Hollenbach (1999) suggest that a significant fraction of planetary systems may be affected in such a way. It is possible that Fomalhaut and the other truncated remnant discs were formed in a similar cluster, and the present structure reflects their formation environment. By implication, the β Pic disc, with its more gradual density fall-off, formed in a more benign environment.

Deeper images of the outer regions of these rings would be of interest to investigate their boundary structures. More extensive modelling of planet-induced resonances, including collisional dust cascades as well as P–R drag, are required in order to explain the grain size, as well as the ring and non-axisymmetric structures seen around these main-sequence stars. This may provide a method of indirectly detecting the presence of low-mass planets.

4 CONCLUSIONS

The results of modelling the spectral energy distributions and the submillimetre images of the dust around Fomalhaut, Vega, ϵ Eridani and β Pictoris have been presented. In the former three cases, the best-fitting models are those of dust rings of average radii ranging from 65 to 120 au, a relatively small radial extent, and abrupt inner and outer boundaries. β Pictoris shows a significantly larger radial extent, with a power-law density distribution. Direct estimates from the SED and mapping indicate grain sizes of 10–100 μm, opacity indices between 0.8 and 1.1, and temperatures of 35–80 K. There does not appear to be a large range of dust temperature within any individual object.

The grain lifetimes are determined mainly by their mutual collisions, and the observed dust is probably formed through collisions of millimetre-sized bodies. We suggest that the large grains are confined to the observed narrow ring structures by planets of a few Earth masses.

ACKNOWLEDGMENTS

The James Clerk Maxwell Telescope is operated by the Joint Astronomy Centre on behalf of the United Kingdom Particle Physics and Astronomy Research Council, the Netherlands Organization for Scientific Research, and the National Research Council of Canada. We thank the referee for useful suggestions.

REFERENCES

Artymowicz P., 1996, in Käufl H. U., Siebenmorgen R., eds, The Role of Dust in the Formation of Stars. Springer, Berlin, p. 137
Augereau J. C., Lagrange A. M., Mouillet D., Papaloizou J. C. B., Grorod P. A., 1999, A&A, 348, 557
Aumann H. H., 1985, in Papagiannis M. D., ed., Proc. IAU Symp. 112, The Search for Extraterrestrial Life: Recent Developments. Reidel, Dordrecht, p. 43
Aumann H. H. et al., 1984, ApJ, 278, L23
Backman D. E., Paresce F., 1993, in Levy E. H., Lunine J. I., eds, Protostars and Planets III. Univ. Arizona Press, Tucson, p. 1253
Barrado y Navascués D., 1998, A&A, 339, 831
Chini R., Krügel E., Kreysa E., 1990, A&A, 227, L5
Chini R., Krügel E., Shustov B., Tutukov A., Kreysa E., 1991, A&A, 252, 220
Dent W. R. F., 1988, ApJ, 325, 252
Dent W. R. F., Greaves J., Mannings V., Coulson I. M., Walther D. M., 1995, MNRAS, 277, L25
Dominik C., Laureijs R. J., Jourdain de Muizon M., Habing H. J., 1998, A&A, 329, L53
Fajardo-Acosta S. B., Telesco C. M., Knacke R. F., 1998, ApJ, 115, 2101
Gillett F. C., 1986, in Israel F. P., ed., Light on Dark Matter. Reidel, Dordrecht, p. 61
Greaves J. S. et al., 1998, ApJ, 506, L133
Gulliver A. F., Hill G., Adelman S. J., 1994, ApJ, 429, L81
Harper D. A., Loewenstein R. F., Davidson J. A., 1984, ApJ, 285, 808
Harvey P. M., Smith B. J., DiFrancesco J., Colome C., Low F. J., 1996, ApJ, 471, 973
Heinrichsen I., Walker H. J., Klaas U., 1998, MNRAS, 293, L78
Heinrichsen I., Walker H. J., Klaas U., Sylvester R. J., Lemke D., 1999, MNRAS, 304, 589
Holland W. S. et al., 1998, Nat, 392, 788

Jewitt D., Matthews H., 1999, AJ, 117, 1056
Jewitt D., Luu J., Chen J., 1996, AJ, 112, 1225
Kalas P., Jewitt D., 1995, AJ, 110, 794
Knacke R. F., Fajardo-Acosta F. B., Telesco C. M., Hackwell J. A., Lynch D. K., Russell R. W., 1993, ApJ, 418, 440
Koerner D. W., Ressler M. E., Werner M. W., Backman D. E., 1998, ApJ, 503, L83
Krügel E., Siebenmorgen R., 1996, in Käufl H. U., Siebenmorgen R., eds, The Role of Dust in the Formation of Stars. Springer, Berlin, p. 262
Li A., Greenberg J. M., 1998, A&A, 331, 291
Lin D. N. C., Papaloizou J., 1986, ApJ, 309, 846
Liou J-C., Zook H. A., 1999, AJ, 118, 580
Liou J.-C., Zook H. A., Dermott S. F., 1996, in Gustafson B. A. F., Hanner M. S., eds, ASP Conf. Ser. Vol. 104, Physics, Chemistry, and Dynamics of Interplanetary Dust. Astron Soc. Pac., San Francisco, p. 163
McCaughrean M. J., O'Dell C. R., 1996, AJ, 111
Mannings V., Barlow M. J., 1998, ApJ, 497, 330
Mathis J. S., Rumpl W., Nordsieck K. H., 1977, ApJ, 217, 425
Mauron N., Dole H., 1998, A&A, 337, 808
Pantin E., Lagage P. O., Artymowicz P., 1997, A&A, 327, 1123
Roques F., Scholl H., Sicardy B., Smith B. A., 1994, Icarus, 108, 37
Saar S. H., Osten R. A., 1997, MNRAS, 284, 803
Schneider G. et al., 1999, ApJ, 513, L127
Smith B. A., Terrile R. J., 1984, Sci, 226, 1421
Stauffer J. R., Hartmann L., Barrado y Navascués D., 1995, ApJ, 454, 910
Stern S. A., Colwell J. E., 1997, AJ, 114, 841
Störzer H., Hollenbach D., 1999, ApJ, 515, 669
Sylvester R. J., Skinner C. J., 1996, MNRAS, 283, 457
Telesco C. M., Knacke R. F., 1991, ApJ, 372, L29
Trilling D. E., Brown R. H., 1998, Nat, 395, 775
van der Bliek N. S., Prusti T., Waters L. B. F. M., 1994, A&A, 285, 229
Zuckerman B., Becklin E. E., 1993, ApJ, 414, 793

This paper has been typeset from a TEX/LATEX file prepared by the author.